

Stability Dependence and Diurnal Change of Large-Scale Turbulence Structures in the Near-Neutral Atmospheric Boundary Layer Observed from a Meteorological Tower

Mitsuaki Horiguchi · Taiichi Hayashi · Ahoro Adachi · Shigeru Onogi

M. Horiguchi · T. Hayashi

Disaster Prevention Research Institute,

Kyoto University, Gokanoshō, Uji, Kyoto, Japan

Tel.: +81-774-38-4161

Fax.: +81-774-38-4158

e-mail: horiguchi@storm.dpri.kyoto-u.ac.jp

A. Adachi · S. Onogi

Meteorological Research Institute,

Japan Meteorological Agency, Tsukuba, Ibaraki, Japan

Abstract Based on the analysis of observations from a 213-m tall meteorological tower at Tsukuba, Japan, we have investigated the favourable conditions for the predominant existence of large-scale turbulence structures in the near-neutral atmospheric boundary layer (ABL). From the wavelet variance spectrum for the streamwise velocity component (u) measured by a sonic anemometer-thermometer at the highest level (200 m), large-scale structures (time-scale range of 100–300 s) predominantly exist under slightly unstable and close to neutral conditions. The emergence of large-scale structures also can be related to the diurnal evolution of the ABL. The large-scale structures play an important role in the overall flow structure of the lower boundary layer. For example, u velocity components at the 200-m and 50-m levels show relatively high correlation with the existence of large-scale structures. Under slightly unstable (near-neutral) conditions, a low-speed region in advance of the high-speed structure shows a positive deviation of temperature and appears as the plume structure that is forced by buoyancy in the heated lower layer. In spite of the difference in buoyancy effects between the near-neutral and unstable cases, large-scale structures are frequently observed in both cases and the same vertical correlation of u components is indicated. However, the vertical wind shear is smaller in the unstable cases. On the other hand, in near-neutral cases, the transport efficiency of momentum at the higher level and the flux contribution of sweep motions are larger than those in the unstable cases.

Keywords *Atmospheric boundary layer · Coherent structures · Momentum transfer · Plume structure · Wavelet transform*

1 Introduction

Laboratory experiments (e.g. Kline et al. 1967; Corino and Brodkey 1969) have

demonstrated the existence of coherent structures in turbulence and their large contributions to the production of new turbulence and turbulent transfer. Coherent structures are well organized and relatively stable long-living eddy structures (Foken 2008). In Barthlott et al. (2007), the term “coherent” is used to denote a distinct “large-scale” fluctuation pattern that is regularly observed in a given turbulent flow.

In the case of the atmospheric boundary layer (ABL), conditions are very different from those in the laboratory, because the Reynolds number of ABL flow is very high ($Re \approx 10^8$). Microfrontal structures (Gao et al. 1989, 1992; Mahrt and Howell 1994), which have been found in field experiments in the surface layer and contain distinct high-speed regions, are one type of coherent structure in the ABL. Streak structures in the streamwise direction close to the ground with organized regions of high-speed and low-speed fluid, which were revealed by large-eddy simulation (LES) models (Deardorff 1972; Lin et al. 1996) and Doppler lidar observations (Drobninski et al. 2004, 2007), are another type of coherent structure. The high-speed streak may contain the aforementioned microfrontal structure. In the ABL, many types of coherent structures have been observed under a variety of atmospheric stability conditions (Lu and Fitzjarrald 1994; Barthlott et al. 2007). Because of the difficulty of measurement, turbulence structures at higher levels in the ABL have not been investigated in detail from observations.

The “neutral” boundary layer is defined for conditions under which the mechanical (shear) production of turbulent kinetic energy is much larger than the buoyant production (e.g. Stull 1988). The neutral ABL has been an important topic of research because the mechanical production (which normally acts in the neutral ABL) is a primary mechanism, especially in the surface layer. Turbulence structures in such a neutral boundary layer with small buoyancy effects are expected to have different geometric aspects from those in the stable or unstable boundary layer (cf. Carper and Porté-Agel 2004). From theoretical considerations and experimental data, Hunt and Morrison (2000) suggested that the dominant mechanism for the neutrally stratified turbulent boundary layer at very high Reynolds numbers is the impingement of “large-scale eddies” onto the wall. This

“top-down” picture differs from the “bottom-up” instability–surface interaction mechanisms proposed in most previous studies.

Townsend (1961) supposed that the turbulent motion in a layer with equilibrium between energy production and dissipation consists of an “active” component responsible for turbulent transfer and an “inactive” component not relevant to the transfer. Later on, the various atmospheric neutral surface-layer characteristics were explained by Högström et al. (2002) in terms of the “top-down” mechanism. They indicated that “detached eddies” of relatively large scale, which are brought down from above into the surface layer, cause the increase of dimensionless vertical velocity variance with height. Although features (length scale, etc.) of these eddies are similar to “inactive” turbulence, they are a very effective means for momentum transport.

In the near-neutral ABL, Horiguchi et al. (2010, 2012) revealed a descending large-scale region of higher wind speed (at a spatial scale of several hundred metres to approximately 1 km) using Doppler sodar or sonic anemometer-thermometers on a meteorological tower. This is essentially a specific type of coherent structure and usually makes a large contribution to the downward momentum transfer. Moreover, large-scale high-speed structures observed in their study appear to correspond to “large-scale eddies” in Hunt and Morrison (2000), which exert great influence on the turbulence in the lower layer. For the general feature of large-scale structures in the near-neutral case (Horiguchi et al. 2012), the mean interval of time between the structures was obtained in the range 310–890 s, which corresponds to the spatial scale in the range 3,100–8,300 m using Taylor’s frozen turbulence hypothesis. However, favourable conditions for the occurrence and development of large-scale structures could not be found. The aim of the present study is to determine conditions under which large-scale structures predominantly occur in the near-neutral ABL. Therefore, the stability dependence and diurnal change of the large-scale structures are examined. Moreover, the conditionally-averaged pattern of structures and the turbulence features under near-neutral conditions are compared with those under unstable conditions.

2 Observed Data and the Analysis Method

The data and analysis method are almost the same as those in Horiguchi et al. (2012). Here, we describe important issues and additional information.

2.1 Outline of Observed Data

We use the archived data from a 213-m tall meteorological tower at the Meteorological Research Institute (MRI), Japan Meteorological Agency (JMA) in Tsukuba City, Japan (36.1°N, 140.1°E). The surrounding area can be characterized by its generally flat topography and by its complex land usage; the land cover includes crop fields, pine woods and forests, houses or buildings, grass fields, and paddy fields (Hiyama et al. 1995).

Fluctuations in the three velocity components and temperature were measured by sonic anemometer-thermometers (DAT-300, Kaijo Co., Tokyo, Japan) at levels of 10, 25, 50, 100, 150, and 200 m on the tower. Standard meteorological elements were also measured at each level using resistance thermometers, and assorted instrumentation. For the evaluation of stability, the ratio of the observation height z to the Obukhov stability length L is used, viz. z/L . The direction of the mean flow is determined from the original data every 30 min and eddy fluxes of momentum and temperature are calculated over this time. Strictly speaking, the temperature measured by a sonic anemometer-thermometer is what is called the “sonic temperature”, given by

$$T_s = T(1+0.32e/p), \quad (1)$$

where T is the air temperature, e is the vapour pressure, and p is the atmospheric pressure

(Foken, 2008). When air temperature or humidity is low, the difference between the sonic temperature and air temperature is not large. For the calculation of the temperature flux in obtaining z/L , the sonic temperature is used because of no measurement of e fluctuations. Under conditions not far from neutral stability, the value of z/L corresponds to the ratio of the buoyant production of turbulence to its shear production. In this study, the level of 50 m is used for the evaluation of stability, and conditions in the range $|z/L| < 0.2$ are regarded as “near-neutral”.

In our analysis, usually the u velocity component at each level is taken in the same horizontal streamwise direction as the mean wind at 50 m; the w velocity component is taken in the vertical direction. For the analysis of the eddy flux, the u component is taken in the three-dimensional mean streamwise direction and the w component is taken in the upward normal to the mean direction. This method is the same as that of “double rotation” (cf. Foken 2008).

2.2 Cases for the Analysis

Daily files are divided into 30-min data segments and time-averaged statistics are calculated for these parts. Usually, an observational case is made up of seven parts (210 min) with the same stability conditions. When an analysis is made for the observation over almost one day, the period is divided into subcases each having a relatively short period of 150 min (five parts) in order to examine the diurnal change of turbulence structures.

All analyzed cases were selected from the data obtained during the period December 1999–March 2000 (a cold and windy period). Assuming the logarithmic wind profile in near-neutral cases, the roughness length z_0 was determined as in the range of 0.6–2.4 m.

2.3 Data Analysis Method

The analysis method of wavelet transform (cf. Kronland-Martinet et al. 1987) and the related procedures are overviewed in this section. Turbulence structures of various scales are extracted by applying an integral wavelet transform to the time series of data. The wavelet coefficient $T_p(a, b)$ with a scale parameter a and a translation parameter b is obtained using an analyzing wavelet.

For the analyzing wavelet, the “Mexican Hat” wavelet function is employed as in other studies on turbulence (e.g. Gao and Li 1993; Chen and Hu 2003). The time scale defined by the value of $2a$, which is a positive part of this wavelet function, is used for sorting turbulent fluctuations according to the scale. In order to examine the distribution of scales for fluctuations, the wavelet variance spectrum $W(a)$ (Mahrt 1991; Collineau and Brunet 1993) is calculated as follows,

$$W(a) = \int_{-\infty}^{+\infty} |T_p(a, b)|^2 db. \quad (2)$$

The integral wavelet transform is applied to the fluctuations of the u velocity component, which are normalized by the standard deviation in each part and connected over seven parts for an observational case (or five parts for a subcase). The wavelet variance spectrum is examined within the time-scale range of 4–352 s (cf. Fig. 3 in Horiguchi et al. 2012). Although the power spectrum using the Fourier transform gives comparable results, the wavelet variance spectrum can indicate a clear peak (maximum) in the large-scale range. In this analysis, the term “large-scale” is used for the structure having a time scale of 100–300 s. One reason for the difference from the power spectrum is the intrinsic smooth distribution of this wavelet variance spectrum.

3 Results and Discussion

3.1 Comparison of Large-Scale Structures in the Near-Neutral Observational Cases

In Horiguchi et al. (2012), 31 near-neutral cases were selected and referred to as case No. 1–31. First of all, conditions in these cases and the occurrence of large-scale structures are investigated in the present analysis. Since large-scale high-speed structures are likely to have a downward movement from a higher level, the highest measurement level (200 m) is used in order to identify the structures. In 17 cases, the wavelet variance spectrum of the u velocity component at 200 m exhibits a peak (global maximum in 10 cases or local maximum in seven cases) in the large-scale range (* in Table 1). The spectral peak located in the large-scale range indicates that large-scale structures are remarkably seen in the turbulent flow. In Table 1, average values of z/L over seven parts are also shown for comparison of the stability conditions.

Properties of the wavelet variance spectrum for the u component at 200 m in the near-neutral observational cases are obtained as follows:

- (1) in the cases during nighttime (four cases, local time range of 1830–0330) under slightly stable conditions ($z/L > 0$), a peak of the spectrum is not found within the large-scale range;
- (2) under slightly unstable conditions ($z/L < 0$) (16 cases), usually wavelet variance has a spectral peak within the large-scale range or gradually increases with the increase of the time scale;
- (3) a peak in the large-scale range (17 cases in total) is found not only under slightly unstable conditions (10 cases), but also under close to neutral conditions ($0 \leq z/L \leq 0.05$) (seven cases).

In connection with the above item 2, in eight cases under slightly unstable ($z/L < 0$) or close to neutral conditions ($z/L = 0.03$), the wavelet variance gradually increases in the large-scale range and in a range of the larger time scale (more than 300 s) (symbol “–” in Table 1). In these cases, some velocity variation with a very large time scale exists in the turbulent flow at the higher level. To be precise, large variance at the very large time

scale is found only at the levels of 100 m and 200 m.

From the present analysis of near-neutral observational cases, a general conclusion can be drawn: that is, large-scale structures predominantly exist (especially in the global maximum cases) under slightly unstable and close to neutral conditions. The values of z/L are in the range of -0.14 to 0.05 . This also indicates that the buoyancy contribution under unstable conditions is not a unique factor for the predominant existence of large-scale structures. The local time of the global maximum cases under close to neutral conditions (cases No. 20 and 25) is during the late afternoon to early evening (1530–1930 LST). The emergence of large-scale structures is possibly also related to the diurnal evolution of the ABL structure. For the slightly unstable cases, the time is not limited to the above period.

The global maximum or gradual increase of wavelet variance in the large-scale range indicates the significant existence of large-scale structures (18 cases in total). In the case of the local maximum, its variance is not so large. As a next step in the analysis, the role of large-scale structures in the overall flow structure of the lower boundary layer is investigated. The analysis of the two-point space–time correlation of the u component between the higher and lower levels (200–50 m) shows relatively high correlation for the cases with a significant existence of large-scale structures (Table 1). The average value of the maximum correlation coefficient is 0.33 (standard deviation $\sigma = 0.06$) for these cases, whereas the average value is 0.22 ($\sigma = 0.08$) in the other cases. This high correlation with the existence of large-scale structures is attributable to the downward extent of such structures from the higher level.

From the present observations, vertical wind shear in the lower boundary layer is evaluated using the non-dimensional wind shear (S) between the 50-m and 200-m levels,

$$S = (u_2 - u_1)/u_*, \quad (3)$$

where u_1 and u_2 are u components at 50 and 200 m, and u_* is the friction velocity. For the cases with significant existence of large-scale structures (18 cases), the wind shear has a

small average value of 4.6 ($\sigma = 0.8$) (Table 1). In the other cases, the average value is 7.2 ($\sigma = 1.5$). This suggests that streamwise momentum is well mixed vertically with the emergence of large-scale structures, supporting the conclusion of the importance of these structures to the overall flow structure of the lower boundary layer.

3.2 Diurnal Change of Large-Scale Structures under Near-Neutral Conditions

In the above section, we compared the properties of large-scale structures among the near-neutral observational cases, usually on different days and in small shifts of the stability condition. Here, the diurnal change of large-scale structures over almost one day under near-neutral conditions is examined to confirm the favourable conditions for the predominant existence of large-scale structures. We selected February 9, 2000, in which near-neutral conditions continued from 0500 to 2230 local standard time (LST), the longest period among the analyzed days. The weather was clear at 0900 LST and became cloudy at 1500 LST at the nearby Tateno station in Tsukuba City. Figure 1 shows the variation of z/L , friction velocity (u_*), and the u velocity component at the 200-m and 50-m levels on this day. Owing to noisy data, statistical values were not obtained at the beginning of the day. The value of z/L indicates slightly stable conditions ($z/L > 0$) until 0830 LST, and slightly unstable afterwards ($z/L < 0$). From 1630 LST, slightly stable conditions returned. Friction velocity decreased with a corresponding decrease in the u component at 200 m and 50 m during the period of near-neutral stability.

The period under near-neutral stability is divided into subcases each having a period of 150 min (five parts). This period is shorter than that of the near-neutral observational cases in Sect. 3.1 in order to prevent a large change of conditions during a subcase. Properties of large-scale structures are examined for each subcase. Table 2 shows the time scale of the peak (global or local maximum) in the wavelet variance spectrum for the u component at 200 m; average values of z/L are also shown.

In subcases 1 and 2 (0500–1000 LST), in which conditions are slightly stable (on average, $z/L = 0.03$ in subcase 1) or close to neutral ($z/L = -0.01$ in subcase 2), wavelet variance spectra for the u component at all levels indicate no dominant peak in the large-scale range. The local maximum at the time scale of 296 s for the 200-m level in subcase 1 is very small; on the other hand, in subcase 2, a relatively large peak (local maximum) is found at the time scale of 124 s (Fig. 2a). Subsequently, in subcases 3 and 4 (1000–1500 LST), in which conditions are slightly unstable ($z/L = -0.09$ and -0.07), spectra for the u component at the higher levels indicate clear peaks in the large-scale range. For subcase 3, a global maximum is found at the time scale of 160 s for the 200-m level (Fig. 2b), which corresponds to a spatial scale of 1,800 m. A global maximum with a larger time scale is also evident at the lower levels (100 m and 50 m); even so, its time scale gradually decreases. For the next subcase (subcase 4), a global maximum is located at the time scale of 124 s for the 200-m level, while a global maximum at the time scale of 100 s is also found in subcase 5 (1500–1730 LST in the late afternoon), in which stability is close to neutral ($z/L = 0.01$). In the evening (subcases 6 and 7, 1730–2230 LST), in which conditions became slightly stable ($z/L = 0.10$ and 0.11), the spectrum shows no dominant peak in the large-scale range.

This example demonstrates that slightly unstable conditions are favourable for the emergence of large-scale structures in the lower part of the near-neutral ABL, and suggests buoyancy effects on the development of turbulence structures. The related process is discussed in the subsequent section. The large-scale structures substantially exist also in the late afternoon under close to neutral conditions, and the overall flow structure of the lower boundary layer changes according to the emergence of large-scale structures. The space–time correlation of the u component between the 200-m and 50-m levels shows relatively high values for the subcases with the predominant existence of large-scale structures. In subcase 1, the maximum correlation coefficient is 0.20, whereas the value reaches 0.33 and 0.35 in subcases 4 and 5 (Table 2). Moreover, the non-dimensional wind shear between the 50-m and 200-m levels, evaluated using Eq. 3, is

small in subcases 3, 4, and 5 ($S = 3.7, 4.2, 4.5$) with the predominant existence of large-scale structures. This suggests that momentum is well mixed vertically. In the other subcases, the non-dimensional value of wind shear is in the range of 6.1–8.4.

The same analysis is made for other examples on December 7, 1999 and January 21, 2000, in which near-neutral conditions existed for periods 0800–1800 and 0430–1930 LST respectively. These examples also demonstrate that slightly unstable conditions are favourable for the emergence of large-scale structures in the lower part of the near-neutral ABL. The predominant existence of large-scale structures in the late afternoon under close to neutral conditions ($z/L = -0.02$) is also found on January 21. Moreover, the overall flow structure of the lower boundary layer in these examples changed according to the emergence of large-scale structures. The diurnal change of properties of large-scale structures is consistent with the result obtained from the comparison between the near-neutral observational cases (Sect. 3.1).

Over land surfaces, the vertical structure of the ABL evolves with the diurnal cycle (e.g. Stull, 1988), with the largest scale of turbulence structures possibly related to the resultant ABL depth. The ABL (mixed layer) grows in depth on fine days under unstable conditions and reaches its maximum depth in late afternoon. Since we do not have observational information in this study, evaluating a connection between the scale of turbulence structures and the ABL depth is difficult.

3.3 Average pattern of Large-Scale Structures in the Near-Neutral and Unstable Cases

As pointed out in the previous sections, in the lower part of the near-neutral ABL, large-scale structures are frequently observed under slightly unstable conditions. Here, for the purpose of characterizing the large-scale structures in the near-neutral cases, we compare these structures with those, such as the plume structure, that are forced by strong buoyancy in the daytime. Moreover, the related process is presented and discussed.

As a typical near-neutral case, Horiguchi et al. (2012) used the period 1330 to 1700 LST on March 29, 2000 (case 29); the average z/L of -0.05 for this case indicates slightly unstable conditions. From a series of wavelet coefficients for the u velocity component at the 200-m level, high-speed events with local maxima exceeding a threshold value were selected. A conditionally-averaged pattern of fluctuations (denoted by the prime) of the u and w components normalized by their standard deviations (σ_u and σ_w) was then depicted on a time–height cross-section (Fig. 5 in Horiguchi et al. 2012). A descending high-speed structure is recognized from the flow pattern, and in advance of the high-speed structure, an ascending low-speed region (structure) is also revealed. The wind pattern of these structures is the same as that of an ejection-sweep structure for velocity, which was observed (Gao et al. 1989) and computed using LES (Su et al. 1998) for forest canopies. The ejection is a low-speed upward turbulent motion and the sweep is a high-speed downward turbulent motion, while the structure of the ejection and sweep is not necessarily large. Compared to the foregoing observations, the present study reveals the structures over a wide height range.

In addition to the wind pattern, temperature fluctuations normalized by the standard deviation (σ_T) are depicted with a red line at each level (50, 100, and 200 m) (Fig. 3). Since the air temperature decreased slightly during the period of the case, a linear trend is removed for each part. Moreover, σ_T decreases from 0.5 to 0.1 K for each part at 50 m and from 0.4 to 0.1 K at 100 m. In the figure, time zero corresponds to the centre of events, and the time progresses from the right to left (the temporal variation can be converted into the spatial distribution from the mean u). Contours indicate u' values and arrows denote w' values. In the ascending low-speed region, the temperature deviation is positive, corresponding to warm air rising. In this case, normalized T' values reach 1.3 at the 50-m and 100-m levels after the removal of the trend. The same structure is usually recognized (15 cases in total among 16 cases) in the slightly unstable (near-neutral) cases. For simplicity, slightly unstable (near-neutral) cases are sometimes referred to as “near-neutral cases” in this and the next section.

The ascending low-speed region is similar to the plume structure that is forced by buoyancy in the heated lower layer. This plume structure has a diameter and a depth on the order of the surface-layer depth (≈ 100 m); ambient mean flow modifies the plume structure so that the leading edge is diffuse and the trailing edge is sharp (Stull, 1988). Kaimal and Businger (1970) observed the wind speed and temperature during the occurrence of a plume and showed a sharp fall in temperature at the trailing edge (“microfront”). As for the u component, it remains low within much of the plume but increases suddenly just ahead of the front. Measured from a fixed tower, the temperature trace shows a “ramp structure” or sawtooth shape close to the surface in the plume (e.g. Schols 1984).

For the purpose of comparison, unstable cases were selected from the same period as the near-neutral cases. These unstable cases have a period of 210 min (seven parts), during which z/L for each part continues in the range $-2.0 < z/L \leq -0.2$. Since observations were made in a cold and windy period, very unstable conditions ($z/L \leq -2.0$) are rare and not included in the analyzed cases. Mean wind direction, horizontal wind speed, friction velocity (u_*), and the value of z/L at 50 m are listed in Table 3. The time scale of the peak in the wavelet variance spectrum for the u component at 200 m is also shown. These unstable cases are referred to as case U-1–13. Average values of wind speed (5.0 m s^{-1}) and friction velocity (0.58 m s^{-1}) for the unstable cases are smaller than those for the slightly unstable (near-neutral) cases (8.1 and 0.82 m s^{-1}). The difference of wind speed is certainly related to the change of stability.

For a typical unstable case, the case during 1100–1430 LST on February 28, 2000 (case U-8) is selected. Here, the average value of the u component at 200 m (9.0 m s^{-1}) is the largest of all cases and the average $z/L = -0.57$. As in the near-neutral case, the wavelet variance spectrum for the u component is examined. At 200 m, a small local maximum is found at the time scale of 104 s (Fig. 4), corresponding to a spatial scale of 900 m using the mean u . At the lower levels (50–150 m), global maxima are located in the time-scale range slightly smaller than 100 s, indicating that relatively small-scale

structures are dominant. From a series of wavelet coefficients for the u component at 200 m, we select high-speed events (six events) and a conditionally-averaged pattern is constructed (Fig. 5). An ascending low-speed region in advance of a descending high-speed structure is extracted also in this unstable case. In the low-speed region, the temperature deviation is positive; normalized T' values reach 0.8 at 50 m and 0.9 at 100 m after the removal of the trend. During the period of the case, the standard deviation of temperature decreases from 0.4 to 0.2 K for each part at 50 m and from 0.3 to 0.2 K at 100 m. The temperature excess above the mean is comparable with that for the typical near-neutral case (case No. 29).

In this case, under unstable conditions, the low-speed region can be regarded as a plume structure. The trailing edge of the low-speed region is sharp and its downwind tilt with height is large near the surface. Although the temperature excess is not so large in the ascending low-speed region, its value is comparable with that for the convective plume observed by Kaimal and Businger (1970). They showed that the maximum temperature excess is approximately 0.6 K at the height of 22.6 m and the entrainment must account in part for the overall attenuation of the temperature signal at that height.

In a few unstable cases, conditionally-averaged patterns from the same analysis are unclear. The reason can be attributed to the difficulty in detecting events from the u component at 200 m. Even so, an ascending low-speed region with the positive temperature deviation can be recognized in all the unstable cases. The wind and temperature fields are almost the same as the ensemble structure of temperature ramp events under unstable conditions in the surface layer, which was observed from a tower (Wilczak, 1984; Feigenwinter and Vogt, 2005).

As for the near-neutral conditions, turbulence structures in the atmospheric surface layer cause strong convergence in the streamwise direction and strong vertical stretching (Schols and Wartena, 1986). The high-speed structure under near-neutral conditions can induce an ascending region at the downwind side. When the lower portion of the ABL is (slightly) unstably stratified, the air lifted from below becomes warmer than that of the

surroundings and buoyancy effects are active. The interaction of the buoyancy-driven region with the preexisting shear-driven structure may induce a larger motion overall.

As is shown in Figs. 3 and 5, the overall pattern of wind and temperature fields under slightly unstable (near-neutral) conditions is similar to that under unstable conditions. Gao et al. (1989) examined the structural characteristics observed in the layer within and above a forest (in the canopy and surface layer). They found close similarity between the unstable and near-neutral coherent structures, and pointed out that vertical wind shear is the major factor in the creation of these structures. In our study, intrusion of the large-scale high-speed structure from the upper level (above the surface layer) is likely to be a driving process for the whole ejection-sweep structure both under near-neutral and unstable conditions. Even so, under unstable conditions, buoyancy effects are large compared to those under near-neutral conditions; the low value of z/L (under unstable conditions) means that the relatively large heat flux is induced by buoyant convection. Possible difference in turbulence features between the near-neutral and unstable cases is examined in the next section.

3.4 Comparison of Turbulence Features between the Near-Neutral and Unstable Cases

First, the wavelet variance spectra at the lower (50 m) and higher (200 m) levels are compared. For the slightly unstable (near-neutral) cases (16 cases), a peak (global or local maximum) of the spectrum for the u velocity component at 200 m is found usually within the large-scale range (10 cases) (Table 1). These maxima correspond to the spatial scales in the range of 1,430–3,080 m from the mean u . For the 50-m level in the same cases, a spectral peak (global maximum) is positioned over a wide range of time scales from 36 to 320 s (310–2,440 m in the spatial scale).

For the unstable cases (13 cases), a peak of the wavelet variance spectrum for the u component at 200 m is found within the large-scale range in nine cases. These maxima

correspond to the spatial scales in the range of 590–2,020 m. In the other cases (four cases), no peak is found within the large-scale range and the wavelet variance gradually increases with the increase of the time scale. For the 50-m level in the same cases, the spectrum always has a global maximum in the time-scale range of 44–256 s (290–1,630 m in the spatial scale). Figure 4 shows an example case (U-8), in which the spectrum has a small local maximum at 104 s and gradually increases in the time-scale range larger than 172 s for the 200-m level. In contrast, a clear peak (global maximum) is situated at 96 s for the 50-m level. Based on the above examinations, the features in the wavelet variance spectrum for the unstable cases do not largely differ from those for the near-neutral cases. Newsom et al. (2008) estimated integral length scales directly from the spatially resolved velocity retrievals by the dual-Doppler lidar data. The streamwise length scale of the u component under unstable conditions (≈ 900 m) is lower than that under near-neutral conditions (1.6 km). Since their observation period is limited to one day, more data are needed for the detailed comparison with our analysis.

Next, the vertical extent of structures from the higher level towards the lower level and the overall flow structure of the lower boundary layer is compared. The analysis of space–time correlation of the u component between the 200-m and 50-m levels shows a vertical extent of structures. The average value of maximum correlation coefficients is 0.33 ($\sigma = 0.08$) for the unstable cases, which is the same as that for the slightly unstable (near-neutral) cases (0.33, $\sigma = 0.07$). By contrast, for the non-dimensional wind shear between the 50-m and 200-m levels, the average value is 3.1 ($\sigma = 1.0$) for the unstable cases, which is smaller than that for the near-neutral cases (4.6, $\sigma = 1.1$). This represents the convectively well-mixed layer under unstable conditions. In this connection, the correlation coefficient between the u and w components ($r_{uw} = \overline{u'w'}/\sigma_u\sigma_w$) is also examined (the overbar indicates the time average). This value depends on the relative content of “active” turbulence that produces the shear stress τ (Högström 1990), and indicates the transport efficiency of momentum (Li and Bou-Zeid 2011). At the lower level (50 m), the average r_{uw} is almost the same for both cases ($r_{uw} = -0.31$ for the

unstable cases and -0.30 for the near-neutral cases). On the other hand, at the higher level (200 m), the average r_{uw} value of -0.21 for the unstable cases ($\sigma = 0.06$) is, in magnitude, definitely lower than that for the near-neutral cases (-0.31 , $\sigma = 0.04$). Therefore, at this level, momentum is more efficiently transferred towards the lower level in the near-neutral cases.

Based on the acoustic sounding data, Thomas et al. (2006) demonstrated that the degree of vertical coherency increases with the flow evolving from neutral to near-convective conditions. This increase was attributed to the evolution of thermal eddies, although the significant influence was limited to the lower layer (below five times the canopy height). In the present study, the downward extent of structures from the comparatively high level (200 m) is analyzed.

Wilczak (1984) found the specific regions of the large-scale eddy structure in the convective surface layer observed from the Boulder Atmospheric Observatory tower, which act to transport momentum in a counter-gradient direction. Moreover, the intensity of the counter-gradient flux tends to increase with height, so that the magnitude of r_{uw} decreases with height. The basic large-scale eddy circulation is inherently inefficient in the use of velocity fluctuations to transport momentum to the surface, in accordance with the present study. By using LES, Moeng and Sullivan (1994) showed that r_{uw} in the shear-driven ABL is about twice as large as in the buoyancy-driven ABL. This result is likely related to the existence of large negative $u'w'$ in both updraft and downdraft regions in the shear case and only in the few strong updraft regions in the buoyancy case.

Finally, characteristics of the turbulent motion are compared. Instantaneous values of $u'w'$ for the Reynolds shear stress are sorted according to the quadrant in the (u', w') plane: (1) $u' \geq 0, w' \geq 0$, (2) $u' < 0, w' \geq 0$ (ejection), (3) $u' < 0, w' < 0$, and (4) $u' \geq 0, w' < 0$ (sweep) (Wallace et al. 1972; Willmarth and Lu 1972). In these quadrants, ejection and sweep motions contribute to the downward transfer of momentum. The flux fraction is a relative contribution of the motion in each quadrant to the momentum flux by all motions. Raupach (1981) defined the imbalance in the contribution of sweep and ejection motions

to the momentum flux using the difference between the flux fractions,

$$\Delta S_0 = \frac{\overline{u'w'_4} - \overline{u'w'_2}}{\overline{u'w'}}, \quad (4)$$

where $\frac{\overline{u'w'_4}}{\overline{u'w'}}$ and $\frac{\overline{u'w'_2}}{\overline{u'w'}}$ are the flux fractions in quadrants 4 and 2, respectively. Based on analytical considerations, Katul et al. (2006) showed that the imbalance can be predicted from measured profiles of the Reynolds stress and the longitudinal velocity standard deviation. They also indicated that in the outer layer ($(z - d)/\delta > 0.4$), $\Delta S_0 < 0$ and in the neutral surface layer, $\Delta S_0 = 0$, where d is the zero-plane displacement and δ is the ABL height.

In this study, at 50 m and 200 m, $\Delta S_0 < 0$ for all unstable cases and slightly unstable (near-neutral) cases, and the contribution of ejection motions in the unstable cases tends to be more dominant than that in the near-neutral cases. In the unstable cases, the average value of ΔS_0 is -0.34 ($\sigma = 0.21$) at 200 m and -0.22 ($\sigma = 0.06$) at 50 m. On the other hand, in the near-neutral cases, the average ΔS_0 is -0.25 ($\sigma = 0.08$) at 200 m and -0.13 ($\sigma = 0.06$) at 50 m. Therefore, in the unstable cases, the upward air motion (nearly corresponding to the ejection motion) in the plume structure can significantly influence the downward momentum flux. In the near-neutral cases, relatively, the contribution of the downward air motion (sweep motion) is large.

As has been noted, some turbulence features similar to those in the unstable cases can be obtained in the near-neutral cases (under slightly unstable conditions). However, small vertical wind shear is recognized in the unstable cases. On the other hand, in the near-neutral cases, the transport efficiency of momentum at the higher level and the flux contribution of sweep motions are larger than those in the unstable cases. They are important features of the structures under near-neutral conditions and suggestive of the effects of the “large-scale eddies” (Hunt and Morrison 2000).

4 Concluding Remarks

Based on the analysis of data obtained from a meteorological tower, we have investigated the conditions for the predominant existence of large-scale turbulence structures in the lower part of the near-neutral ABL. From the analysis of the streamwise velocity component (u) at the highest level (200 m), large-scale structures predominantly exist under slightly unstable and close to neutral conditions. These large-scale structures play an important role in the overall flow structure of the lower boundary layer. It appears that the development of large-scale structures is inhibited by thermal stratification under (slightly) stable conditions. As for the diurnal change in large-scale structures, the vertical structure of the ABL also evolves and its top level changes with the diurnal cycle. The largest scale of structures is possibly related to the ABL depth; the ABL becomes deep under unstable conditions, also indicating the dependence on stability.

The average pattern of structures under slightly unstable (near-neutral) conditions is similar to that of the plume structure under unstable conditions ($z/L \leq -0.2$). Buoyancy effects are certainly large under unstable conditions. Even so, the intrusion of the large-scale high-speed structure from the upper level is likely to be a driving process for the whole ejection-sweep structure both under near-neutral and unstable conditions. Under near-neutral conditions, momentum is more efficiently transferred at the higher level and the flux contribution of sweep motions is relatively large. Large-scale high-speed structures observed under near-neutral conditions appear to correspond to the “large-scale eddies” that exert great influence on turbulence in the lower part of the boundary layer (Hunt and Morrison 2000). Large-scale high-speed structures also can affect the turbulence features.

Streaks are alternating bands of relatively higher and lower speed flow and parallel to the mean shear direction in the lower part of the ABL. Foster et al. (2006) proposed that the streak motion plays an important role in the maintenance of the surface stress by establishing the preferential conditions for the ejections and sweeps that dominate the

surface stress. As explained above, the large-scale structure in the near-neutral ABL comprises an ejection-sweep structure, and its relationship with the streak is also of particular interest. The present investigation has been focused on the examination of the layer down to the 50 m level. Even so, it is of interest to examine the turbulence characteristics in the layer near the surface. Below the vigorous turbulence layer around the 25-m level, large-scale high-speed structures extend to the lowest level (10 m) (cf. Fig. 3). Turbulence structures of large horizontal scale tend to also have a large vertical scale, and thus exert a great influence on the turbulence in the lower layer. The future direction of this study will be one that investigates the process of strong wind events at the surface.

Acknowledgements The authors would like to thank the members of the MRI for the observations using the meteorological tower and a great deal of support for the research. The first author is also grateful to the colleagues in the Disaster Prevention Research Institute and the members of the Meteorological Society of Japan for fruitful discussions.

References

- Barthlott C, Drobinski P, Fesquet C, Dubos T, Pietras C (2007) Long-term study of coherent structures in the atmospheric surface layer. *Boundary-Layer Meteorol* 125:1–24
- Carper MA, Porté-Agel F (2004) The role of coherent structures in subfilter-scale dissipation of turbulence measured in the atmospheric surface layer. *J Turb N40*
- Chen J, Hu F (2003) Coherent structures detected in atmospheric boundary-layer turbulence using wavelet transforms at Huaihe River basin, China. *Boundary-Layer Meteorol* 107:429–444
- Collineau S, Brunet Y (1993) Detection of turbulent coherent motions in a forest canopy part I: wavelet analysis. *Boundary-Layer Meteorol* 65:357–379
- Corino ER, Brodkey RS (1969) A visual investigation of the wall region in turbulent flow. *J Fluid Mech* 37:1–30
- Deardorff JW (1972) Numerical investigation of neutral and unstable planetary boundary layers. *J Atmos Sci* 29:91–115
- Drobinski P, Carlotti P, Newsom RK, Banta RM, Foster RC, Redelsperger J-L (2004) The structure of the near-neutral atmospheric surface layer. *J Atmos Sci* 61:699–714
- Drobinski P, Carlotti P, Redelsperger J-L, Banta RM, Masson V, Newsom RK (2007) Numerical and experimental investigation of the neutral atmospheric surface layer. *J Atmos Sci* 64:137–156
- Feigenwinter C, Vogt R (2005) Detection and analysis of coherent structures in urban turbulence. *Theor Appl Climatol* 81:219–230
- Foken T (2008) *Micrometeorology*. Springer-Verlag, Berlin Heidelberg 306 pp
- Foster RC, Vianey F, Drobinski P, Carlotti P (2006) Near-surface coherent structures and the vertical momentum flux in a large-eddy simulation of the neutrally-stratified boundary layer. *Boundary-Layer Meteorol* 120:229–255
- Gao W, Li BL (1993) Wavelet analysis of coherent structures at the atmosphere–forest interface. *J Appl Meteorol* 32:1717–1725
- Gao W, Shaw RH, Paw UKT (1989) Observation of organized structure in turbulent flow within and above a forest canopy. *Boundary-Layer Meteorol* 47:349–377
- Gao W, Shaw RH, Paw UKT (1992) Conditional analysis of temperature and humidity microfronts and ejection/sweep motions within and above a deciduous forest. *Boundary-Layer Meteorol* 59:35–57

- Hiyama T, Sugita M, Kayane I (1995) Variability of surface fluxes within a complex area observed during TABLE 92. *Agric For Meteorol* 73:189–207
- Högström U (1990) Analysis of turbulence structure in the surface layer with a modified similarity formulation for near neutral conditions. *J Atmos Sci* 47:1949–1972
- Högström U, Hunt JCR, Smedman A-S (2002) Theory and measurements for turbulence spectra and variances in the atmospheric neutral surface layer. *Boundary-Layer Meteorol* 103:101–124
- Horiguchi M, Hayashi T, Adachi A, Onogi S (2012) Large-Scale turbulence structures and their contributions to the momentum flux and turbulence in the near-neutral atmospheric boundary layer observed from a 213-m tall meteorological tower. *Boundary-Layer Meteorol* 144:179–198
- Horiguchi M, Hayashi T, Hashiguchi H, Ito Y, Ueda H (2010) Observations of coherent turbulence structures in the near-neutral atmospheric boundary layer. *Boundary-Layer Meteorol* 136:25–44
- Hunt JCR, Morrison JF (2000) Eddy structure in turbulent boundary layers. *Eur J Mech B* 19:673–694
- Kaimal JC, Businger JA (1970) Case studies of a convective plume and a dust devil. *J Appl Meteorol* 9:612–620
- Katul G, Poggi D, Cava D, Finnigan J (2006) The relative importance of ejections and sweeps to momentum transfer in the atmospheric boundary layer. *Boundary-Layer Meteorol* 120:367–375
- Kline SJ, Reynolds WC, Schraub FA, Runstadler PW (1967) The structure of turbulent boundary layers. *J Fluid Mech* 30:741–773
- Kronland-Martinet R, Morlet J, Grossmann A (1987) Analysis of sound patterns through wavelet transforms. *Int J Patt Recogn Artif Intell* 1:273–302
- Li D, Bou-Zeid E (2011) Coherent structures and the dissimilarity of turbulent transport of momentum and scalars in the unstable atmospheric surface layer. *Boundary-Layer Meteorol* 140:243–262
- Lin C-L, McWilliams JC, Moeng C-H, Sullivan PP (1996) Coherent structures and dynamics in a neutrally stratified planetary boundary layer flow. *Phys Fluids* 8:2626–2639
- Lu C-H, Fitzjarrald DR (1994) Seasonal and diurnal variations of coherent structures over a deciduous forest. *Boundary-Layer Meteorol* 69:43–69
- Mahrt L (1991) Eddy asymmetry in the sheared heated boundary layer. *J Atmos Sci* 48:472–492
- Mahrt L, Howell JF (1994) The influence of coherent structures and microfronts on scaling laws using global and local transforms. *J Fluid Mech* 260:247–270
- Moeng C-H, Sullivan PP (1994) A comparison of shear- and buoyancy-driven planetary boundary layer flows. *J Atmos Sci* 51:999–1022
- Newsom R, Calhoun R, Ligon D, Allwine J (2008) Linearly organized turbulence structures observed over a suburban area by dual-Doppler lidar. *Boundary-Layer Meteorol* 127:111–130
- Raupach MR (1981) Conditional statistics of Reynolds stress in rough-wall and smooth-wall turbulent boundary layers. *J Fluid Mech* 108: 363–382
- Schols JLJ (1984) The detection and measurement of turbulent structures in the atmospheric surface layer. *Boundary-Layer Meteorol* 29:39–58
- Schols JLJ, Wartena L (1986) A dynamical description of turbulent structures in the near neutral atmospheric surface layer: the role of static pressure fluctuations. *Boundary-Layer Meteorol* 34:1–15
- Stull RB (1988) *An introduction to boundary layer meteorology*. Kluwer Academic Publishers, Dordrecht 670 pp
- Su H-B, Shaw RH, Paw UKT, Moeng C-H, Sullivan PP (1998) Turbulent statistics of neutrally stratified flow within and above a sparse forest from large-eddy simulation and field observations. *Boundary-Layer Meteorol* 88:363–397
- Thomas C, Mayer J-C, Meixner FX, Foken T (2006) Analysis of low-frequency turbulence above tall vegetation using a Doppler sodar. *Boundary-Layer Meteorol* 119:563–587
- Townsend AA (1961) Equilibrium layers and wall turbulence. *J Fluid Mech* 11:97–120
- Wallace JM, Eckelmann H, Brodkey RS (1972) The wall region in turbulent shear flow. *J Fluid Mech* 54: 39–48
- Willmarth WW, Lu SS (1972) Structure of the Reynolds stress near the wall. *J Fluid Mech* 55: 65–92
- Wilczak JM (1984) Large-scale eddies in the unstably stratified atmospheric surface layer. Part I: velocity and temperature structure. *J Atmos Sci* 41:3537–3550

Table 1 Time scale of the peak in the wavelet variance spectrum for the u component at 200 m. The analysis is made for near-neutral observational cases.

Case No.	Date	Time (LST)	Average z/L	Time scale of the peak in the wavelet variance spectrum (s)		Maximum correlation coefficient	Wind shear, S
				Global maximum	Local maximum		
1	3 Dec 1999	0730–1100	0.00	72		0.32	5.5
2	3 Dec 1999	1230–1600	−0.04	–	28	0.37	4.3
3	7 Dec 1999	1330–1700	−0.01	80		0.36	5.2
4	12 Dec 1999	1000–1330	−0.13	236 ^a		0.35	3.0
5	26 Dec 1999	1430–1800	0.03	44	232 ^a	0.22	6.4
6	4 Jan 2000	1230–1600	−0.09	–	48	0.37	3.9
7	11 Jan 2000	1230–1600	−0.08	–	80	0.37	3.9
8	20 Jan 2000	1330–1700	−0.03	–	52, 156 ^a	0.37	5.5
9	20 Jan 2000	1830–2200	0.08	28		0.10	8.3
10	21 Jan 2000	1430–1800	0.00	72	240 ^a	0.30	5.5
11	31 Jan 2000	1500–1830	0.03	–	108 ^a	0.28	5.3
12	9 Feb 2000	0600–0930	0.01	24		0.18	6.1
13	10 Feb 2000	0000–0330	0.11	16		0.17	10.5
14	10 Feb 2000	0630–1000	−0.04	40	316	0.12	8.1
15	16 Feb 2000	1530–1900	0.03	44		0.27	6.8
16	21 Feb 2000	1430–1800	−0.02	140 ^a		0.25	4.7
17	22 Feb 2000	1400–1730	−0.04	112 ^a		0.31	4.5
18	29 Feb 2000	0630–1000	−0.07	180 ^a	60	0.22	5.4
19	29 Feb 2000	1600–1930	0.03	–	20, 84	0.24	6.1
20	9 Mar 2000	1600–1930	0.03	220 ^a		0.33	5.2
21	17 Mar 2000	1500–1830	−0.02	–	40, 112 ^a	0.33	4.9
22	18 Mar 2000	1530–1900	0.01	32	124 ^a	0.18	6.8
23	19 Mar 2000	1530–1900	0.03	40	172 ^a	0.14	8.2
24	20 Mar 2000	1430–1800	−0.07	260 ^a		0.36	3.7
25	24 Mar 2000	1530–1900	0.05	196 ^a	40, 76	0.37	5.8
26	26 Mar 2000	1500–1830	−0.05	–		0.46	4.3
27	29 Mar 2000	0000–0330	0.05	24		0.19	7.7
28	29 Mar 2000	0630–1000	−0.05	172 ^a	92	0.33	4.3
29	29 Mar 2000	1330–1700	−0.05	180 ^a	40	0.31	4.4
30	29 Mar 2000	2030–2400	0.06	20		0.27	8.5
31	30 Mar 2000	0830–1200	−0.14	240 ^a		0.36	3.4

Dash (–) means the case when the wavelet variance increases in the large time-scale region. Average values of z/L are also shown. In addition, the maximum correlation coefficient and the non-dimensional wind shear (S) between 200 m and 50 m for the u component are shown

^a Peak of the wavelet variance spectrum within the large-scale range (100–300 s)

Table 2 Time scale of the peak in the wavelet variance spectrum for the u component at 200 m, and the maximum correlation coefficient and the non-dimensional wind shear (S) between 200 m and 50 m for the u component

Subcase No.	Time (LST)	Average z/L	Time scale of the peak in the wavelet variance spectrum (s)		Maximum correlation coefficient	Wind shear, S
			Global maximum	Local maximum		
1	0500–0730	0.03	20	296	0.20	6.4
2	0730–1000	−0.01	24	124	0.22	6.1
3	1000–1230	−0.09	160		0.25	3.7
4	1230–1500	−0.07	124		0.33	4.2
5	1500–1730	0.01	100		0.35	4.5
6	1730–2000	0.10	40		0.18	8.0
7	2000–2230	0.11	68	28	0.20	8.4

The analysis is made for subcases on February 9, 2000. Average values of z/L are also shown

Table 3 Mean wind directions (for seven parts) and average values of horizontal wind speed, friction velocity (u_*), and z/L at 50 m for the unstable cases

Case No.	Date	Time (LST)	Wind direction (°)	Horizontal wind speed (m s^{-1})	u_* (m s^{-1})	z/L	Time scale of the peak in the wavelet variance spectrum (s)	
							Global maximum	Local maximum
1	8 Dec 1999	1000–1330	300–343	3.0	0.50	−0.69	252	28, 108
2	21 Dec 1999	0830–1200	244–272	3.9	0.46	−0.47	–	
3	25 Dec 1999	1130–1500	274–310	2.9	0.38	−0.72	264	56
4	22 Jan 2000	0830–1200	240–307	3.9	0.47	−0.69	–	48, 116
5	26 Jan 2000	0900–1230	305–318	6.5	0.64	−0.29	240	
6	18 Feb 2000	1000–1330	279–333	6.9	0.75	−0.32	–	
7	23 Feb 2000	0930–1300	295–319	4.5	0.56	−0.80	196	76
8	28 Feb 2000	1100–1430	183–204	6.8	0.65	−0.57	–	104
9	1 Mar 2000	0900–1230	287–320	4.0	0.61	−0.61	–	80
10	10 Mar 2000	1130–1500	280–314	7.2	0.80	−0.33	–	
11	11 Mar 2000	1300–1630	190–215	4.4	0.50	−0.58	232	20
12	19 Mar 2000	1130–1500	180–220	4.3	0.51	−0.60	196	60
13	27 Mar 2000	0830–1200	259–297	6.3	0.74	−0.39	144	

The time scale of the peak in the wavelet variance spectrum for the u component at 200 m is also shown. Dash (–) means the case when wavelet variance increases in the large time-scale region

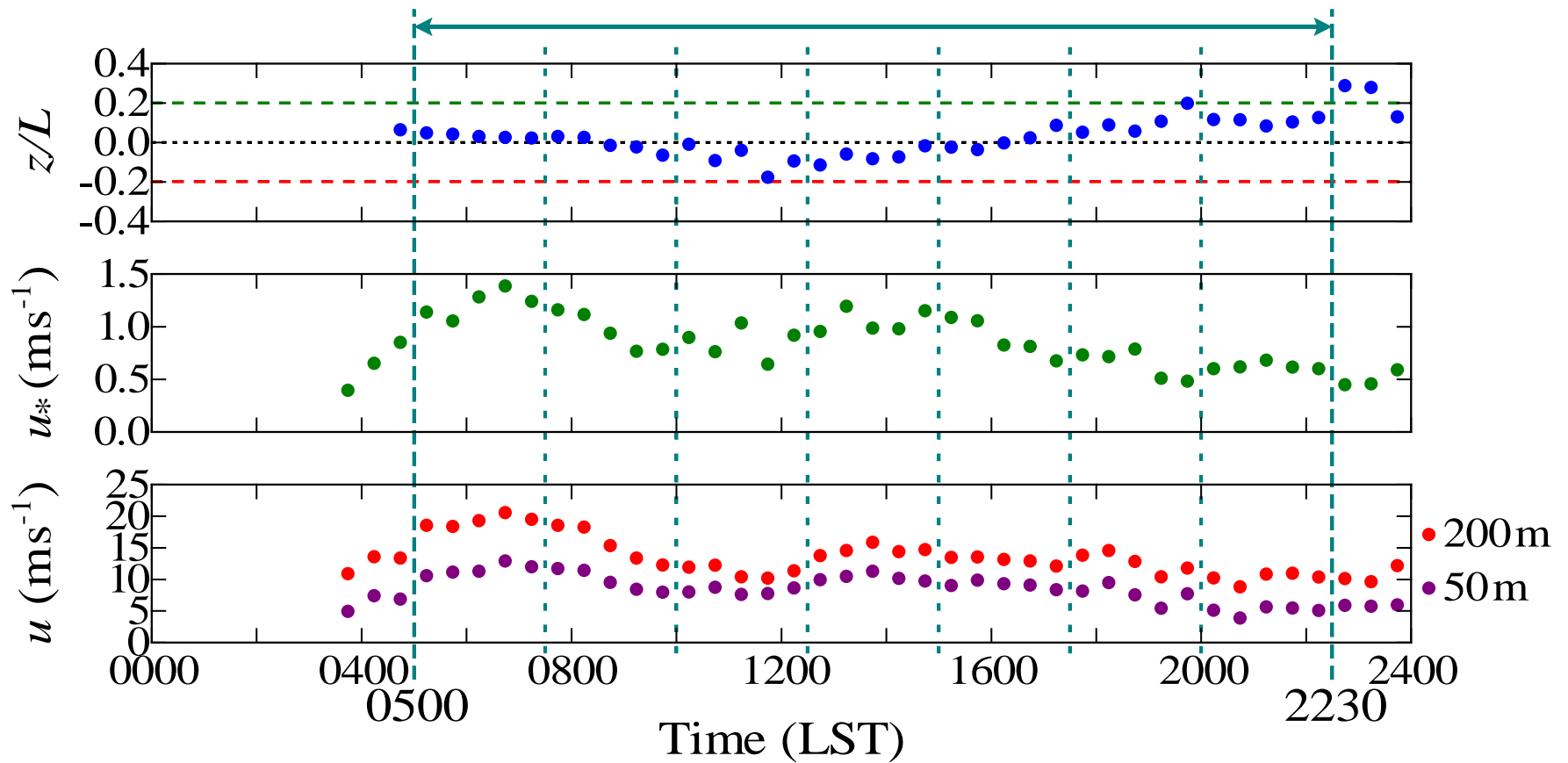


Fig. 1 z/L , friction velocity (u_*), and u velocity components at 200 m and 50 m on February 9, 2000. Periods for the analysis (0500–2230) and subcases (each 150 min) are also shown

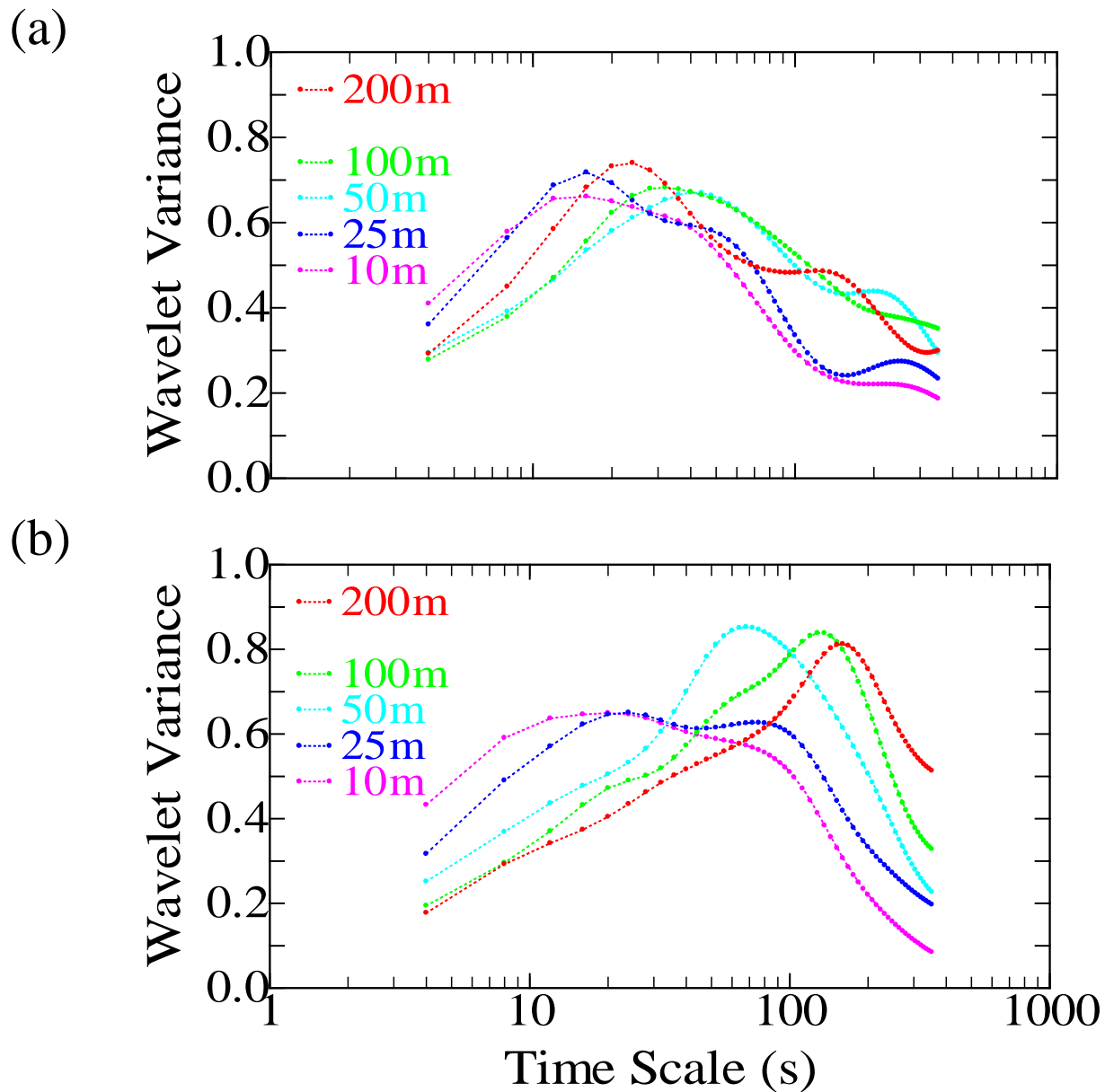


Fig. 2 Wavelet variance spectra of the u velocity component as a function of the time scale for the subcases during 0730–1000 (a) and 1000–1230 LST (b) on February 9, 2000. The data at the 150-m level were not obtained

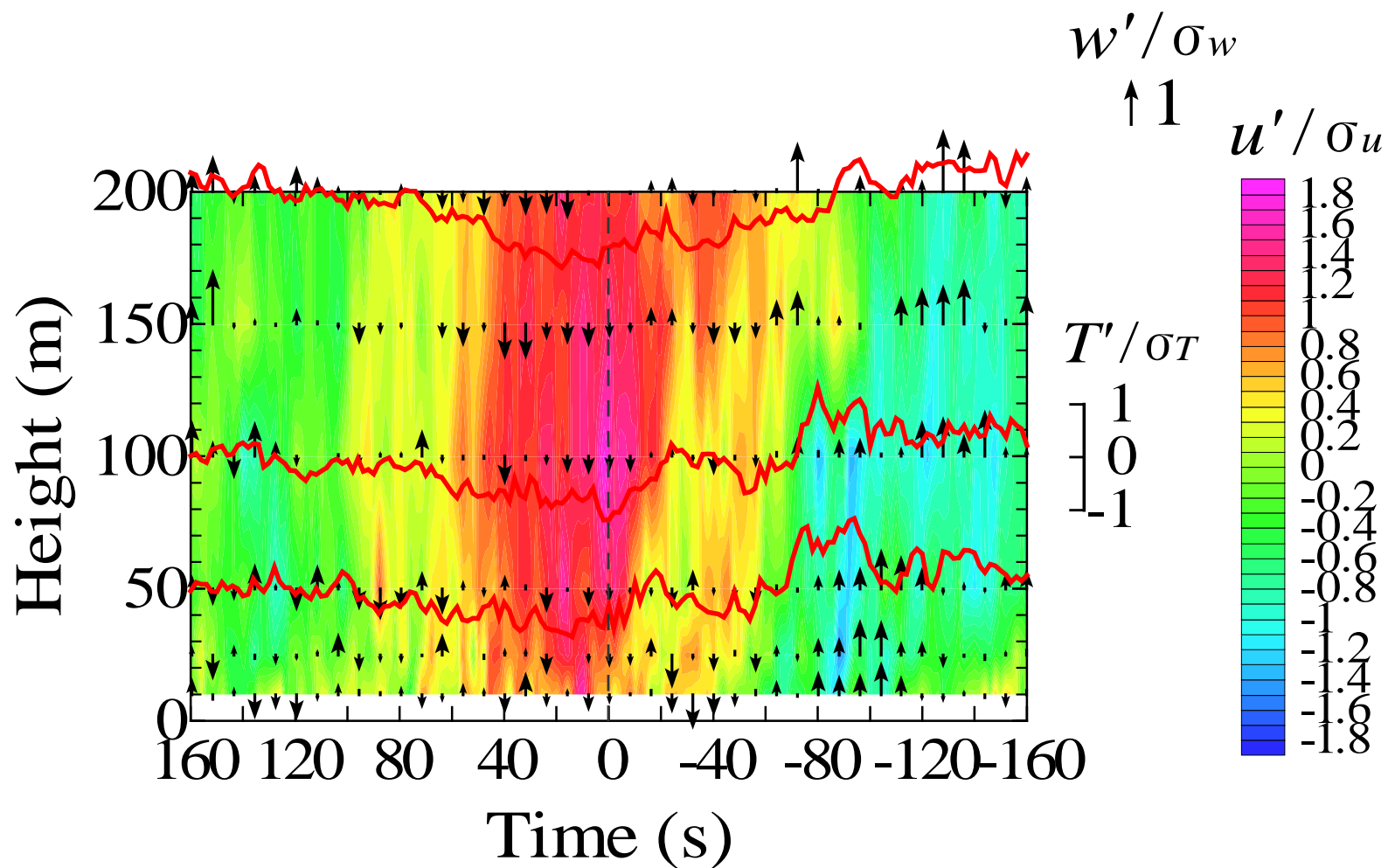


Fig. 3 Conditionally-averaged wind pattern on a time–height cross-section (zero corresponds to the time of the events) for the near-neutral case during 1330–1700 LST on March 29, 2000. Contours indicate normalized u' values and arrows denote normalized w' values. The red line at each level shows the normalized value of the temperature deviation. Based on Fig. 5 in Horiguchi et al. (2012)

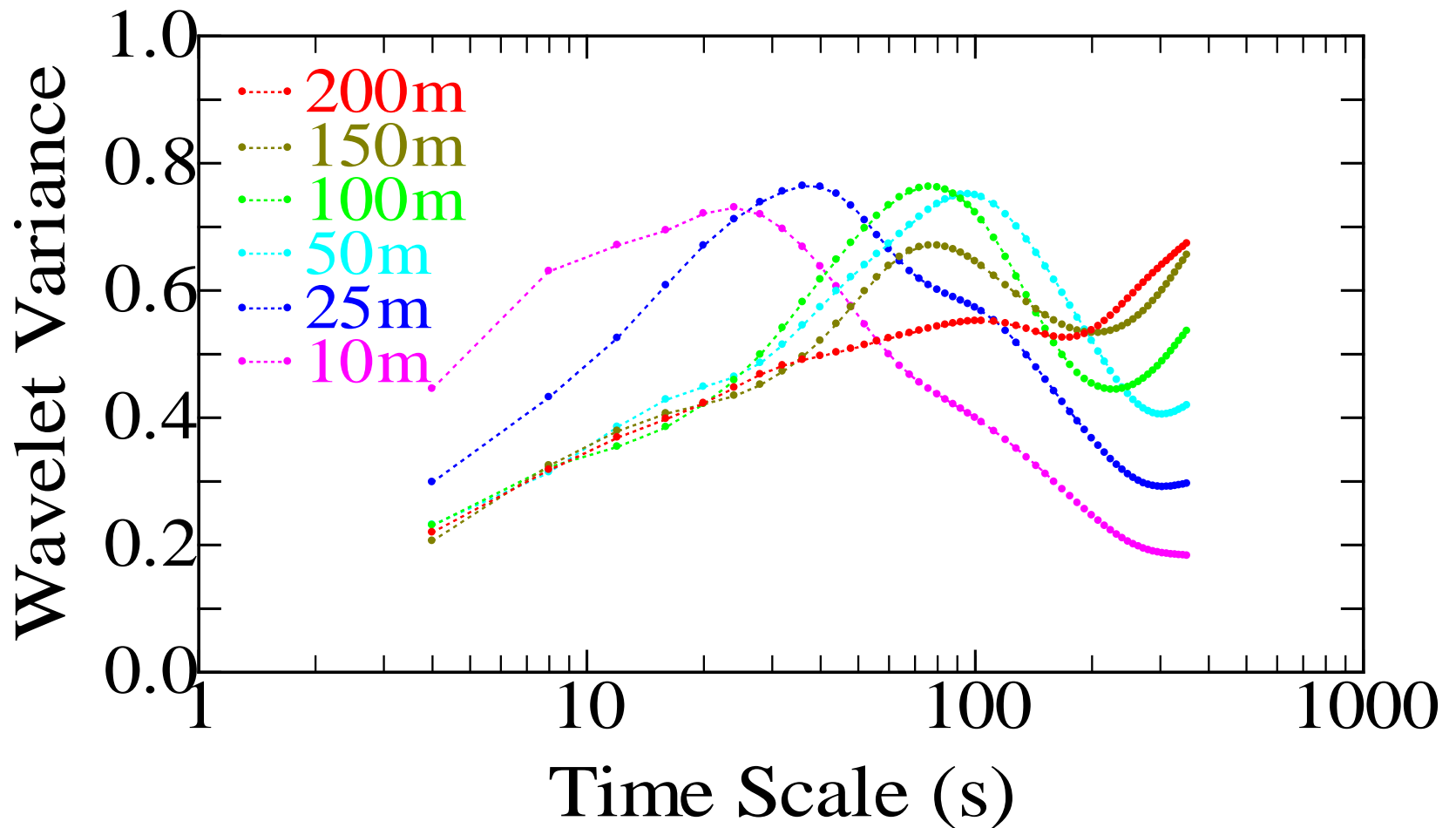


Fig. 4 Wavelet variance spectra of the u velocity component as a function of the time scale for the unstable case during 1100–1430 LST on February 28, 2000

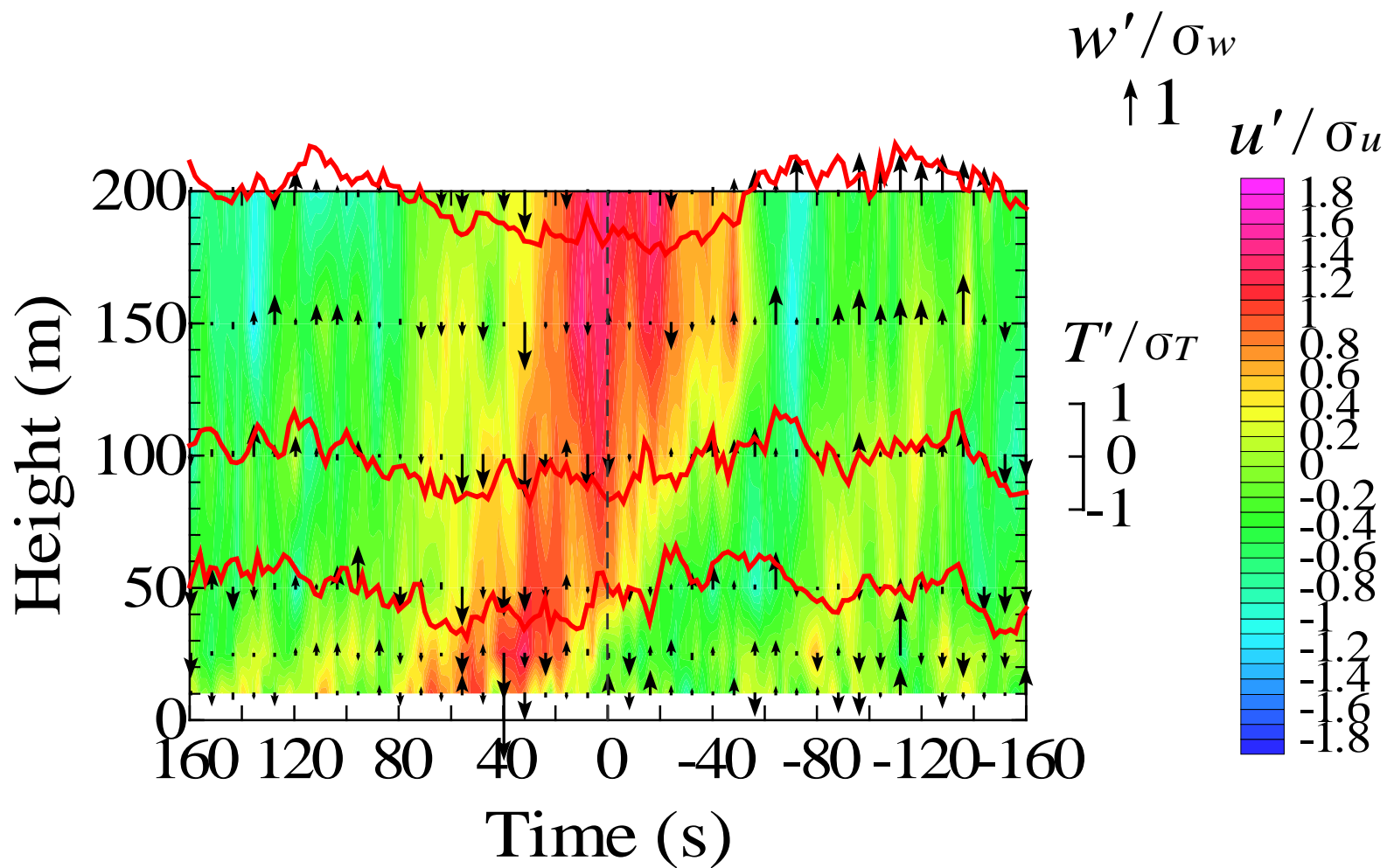


Fig. 5 As Fig. 3, but for the unstable case during 1100–1430 LST on February 28, 2000